

Graph and Simplicial Complex Prediction Gaussian Process via the Hodgelet Representations

Mathieu Alain^{1†} So Takao² Bastian Rieck³ Xiaowen Dong⁴ Emmanuel Noutahi⁵

¹University College London ²California Institute of Technology ³University of Fribourg

⁴University of Oxford ⁵Valence Labs

[†]mathieu.alain.21@ucl.ac.uk

Abstract

Predicting the labels of graph-structured data is crucial in scientific applications and is often achieved using graph neural networks (GNNs). However, when data is scarce, GNNs suffer from overfitting, leading to poor performance. Recently, Gaussian processes (GPs) with graph-level inputs have been proposed as an alternative. In this work, we extend the Gaussian process framework to simplicial complexes (SCs), enabling the handling of edge-level attributes and attributes supported on higher-order simplices. We further augment the resulting SC representations by considering their Hodge decompositions, allowing us to account for homological information, such as the number of holes, in the SC. We demonstrate that our framework enhances the predictions across various applications, paving the way for GPs to be more widely used for graph and SC-level predictions.

1 Introduction

In recent years, considerable efforts have been made in adapting machine learning to non-Euclidean domains such as graphs [Bronstein et al., 2021, Papamarkou et al., 2024]. This departure from the Euclidean setting presents challenges due to the irregularity, varying sizes, and multi-site information (e.g. vertices and edges) inherent to these objects. Predicting labels, whether continuous or discrete, from graph-structured data is crucial in many scientific and industrial applications. This task can range from estimating the properties of molecules according to their chemical structures to classifying documents. Simplicial complexes (SCs) are a generalisation of graphs that include polyadic interactions. Rather than limiting interactions to only those along edges, SCs use simplices to express interactions among an arbitrary number of vertices. Of particular interest are simplicial 2-complexes, which can be seen as graphs extended to include 2-simplices, that is, triangular faces (triangles for short) formed by adjacent vertices. Among their many applications, they can represent two-dimensional meshes [Ballester et al., 2024] and triadic protein–protein interaction networks.

Graph neural networks (GNNs) are generally the model of choice for graph-level classification tasks. However, their main disadvantages are that: (1) they often require large datasets for effective training, (2) their predictions can be difficult to interpret, despite growing efforts in developing GNN explainability methods [Yuan et al., 2021, Ying et al., 2019, Luo et al., 2020], and (3) they are prone to overfitting. On the other hand, many graph kernels [Borgwardt et al., 2020] struggle with scalability, high-dimensional attributes, or require handcrafted features to handle varying graph sizes effectively. A workaround is to use classical Euclidean kernels, however, this raises the challenge of constructing a robust representation vector for each graph that effectively captures both its topological structure and its attributes. Assuming such representations exist, they can be effortlessly employed alongside Gaussian Processes (GPs) [Rasmussen and Williams, 2005] to predict their labels; GPs are data-efficient, non-parametric and interpretable models, which makes them attractive, especially in a small-to-medium data regime. In addition, any parameters used to generate the representation can

be tuned alongside the hyperparameters of the kernel by maximising the marginal likelihood, thus offering a principled alternative to validation-based tuning (though cross-validation remains useful for model selection and assessing generalisation).

A promising approach to capture information from the vertex attributes of a graph while preserving its topological structure is to leverage techniques from graph signal processing [Ortega et al., 2018] and, in particular, the flexible (graph) wavelet transform [Hammond et al., 2011]. The essence of this technique is to compute the wavelet coefficients by applying the wavelet transform to the vertex attributes of each graph. In Opolka et al. [2023], the authors use these coefficients to design graph representations that are fed as inputs to classical GPs, e.g. the radial basis function (RBF) GP. The wavelet transform parameters are then optimised in conjunction with the kernel hyperparameters; by learning the wavelet parameters, it becomes possible to highlight certain frequencies present in the graph-structured data, allowing them to extract the most relevant information from the attributes for a given task. While their method can reliably handle the vertex attributes of a graph, it does not take into account the edge attributes. In the context of graph label prediction, this constitutes an important limitation, since the edge attributes can contain valuable information, for example, flow magnitudes, interaction strengths, or binding affinities.

This critical shortcoming motivates us to explore the simplicial complex wavelet transform [Barbarossa and Sardellitti, 2020] as a way to generate graph representations that can accept both vertex and edge attributes — unlike the Fourier transform, the wavelet transform offers the advantage of simultaneous localisation in space and frequencies. We further use the Hodge decomposition to express these coefficients into three components — exact, co-exact, and harmonic — which respectively characterise signals that are “non-rotational,” “non-divergent”, and “neither rotational nor divergent”. We refer to our representations constructed from these coefficients as the Hodgelet representations. Previous studies have shown that decomposing a signal and treating each component separately can significantly improve the predictive performance of a model [Barbarossa and Sardellitti, 2020, Battiloro et al., 2023, Yang et al., 2024, Isufi et al., 2025]. This can be explained by the explicit topological description provided by the Hodge decomposition. For example, the harmonic subspace gives knowledge about the number of holes or connected components. This type of information is often valuable for prediction tasks, as it captures key characteristics of the SC.

Contributions. Our paper seeks to demonstrate that enhancing graph representations for GPs can be achieved by: (1) incorporating edge attributes (and if available, other higher-order simplex attributes) through the SC wavelet transform and (2) decomposing these attributes into their corresponding Hodge components. We primarily focus on simplicial 2-complexes, consisting of vertices, edges and triangles, as these are sufficient for most applications. Nevertheless, our approach introduced in this paper can be implemented for SCs of any finite dimension, and even for more general structures like cellular complexes [Alain et al., 2024a] and hypergraphs. Finally, although our framework is well-suited for GPs — the marginal likelihood optimisation provides a convenient strategy for adjusting the wavelet parameters — the Hodgelet representations can be incorporated into other machine learning models. This work is the extension of our workshop paper [Alain et al., 2024b].

2 Simplicial Complex Prediction with Gaussian Processes

In this section, we briefly introduce the concept of simplicial complex and establish the framework for predicting their labels using Gaussian processes.

2.1 Simplicial Complexes

We begin by considering the *simplex* set S_k , which consists of N_k k -simplices. Of special interest to us are S_0 , S_1 , and S_2 , which correspond to sets of points, lines, and triangular faces, respectively. Next, we suppose that the sequence $(S_k)_{k=1}^K$ forms a simplicial K -complex (see Figure 1(b)). Needless to say, not all such sequences constitute a *simplicial complex*. We refer the reader to Appendix A and Barbarossa and Sardellitti [2020] for more details. Observe that a graph (see Figure 1(a)) is nothing more than a simplicial 1-complex.

Furthermore, we assume that each k -simplex has a corresponding real-valued *attribute vector* of dimension D_k that is given by some attribute function $S_k \rightarrow \mathbb{R}^{D_k}$. These attributes can be understood as signals on the simplices, a particularly relevant point of view when we present the wavelet transform in Section 4.1.

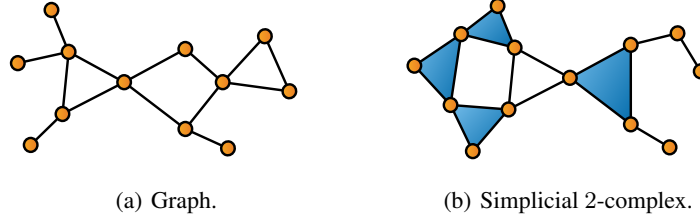


Figure 1: Orange vertices are the 0-simplices, black edges are the 1-simplices, and blue triangles are the 2-simplices.

Next, we fix an orientation on the simplices; the choice of orientation is not important and is typically determined by assigning an ordering on the vertices that form the simplices. This allows us to express the incidence structure of the SC — how the $(k - 1)$ -simplices are connected to the k -simplices — in terms of the signed *incidence matrices* $\mathbf{B}_k \in \mathbb{Z}^{N_{k-1} \times N_k}$. We set $\mathbf{B}_0 := \mathbf{0}$ and $\mathbf{B}_{k>K} := \mathbf{0}$ for notational convenience. Since the simplices are ordered (each of them is assigned a particular index), we can represent the attribute functions using the *attribute matrices* $\mathbf{X}_k \in \mathbb{R}^{N_k \times D_k}$.

Finally, we treat each dimension $1 \leq d \leq D_k$ separately, since they may represent attributes of different nature (e.g. price, length, and colour). The attribute matrices can therefore be expressed as $\mathbf{X}_k := [\mathbf{x}_{k1} \cdots \mathbf{x}_{kD_k}] \in \mathbb{R}^{N_k \times D_k}$, where $\mathbf{x}_{kd} \in \mathbb{R}^{N_k}$ is the attribute vector corresponding to the d -th dimension. For ease of exposition, hereafter, we will only consider the case $D_k = 1$, that is, each simplex only has a scalar attribute, and we denote \mathbf{X}_k simply by \mathbf{x}_k . In this case, every \mathbf{x}_k lives in the *attribute space* \mathbb{R}^{N_k} . Lastly, we express the resulting *attributed simplicial complex* as the sequence $(S_k, \mathbf{x}_k)_{k=1}^K$ of pairs of simplex set and attribute vectors.

2.2 Gaussian Process Prediction of Attributed SCs

Let \mathcal{S} be a set of attributed simplicial K -complexes and \mathcal{Y} be a set of labels. Given a dataset $\mathcal{D} \subseteq \mathcal{S} \times \mathcal{Y}$ composed of m pairs of attributed SC and label, our task is to learn a predictive function $g : \mathcal{S} \rightarrow \mathcal{Y}$. We choose Gaussian processes to model the prediction function [Rasmussen and Williams, 2005]. GPs offer a principled and Bayesian perspective for inferring functions; they are stochastic processes that generalise the concept of Gaussian distribution to function spaces and can provide prior distributions for function-valued random variables.

Inference with GPs proceeds by first considering a latent function $f : \mathcal{S} \rightarrow \mathbb{R}$, distributed according to a GP prior with mean function $\mu : \mathcal{S} \rightarrow \mathbb{R}$ and kernel $\kappa : \mathcal{S} \times \mathcal{S} \rightarrow \mathbb{R}$. We assume that κ has hyperparameters that can be tuned, which provides an advantage over neural network models, as they are generally interpretable. Next, we introduce a likelihood model $p(y | f, S)$, for every $(S, y) \in \mathcal{S} \times \mathcal{Y}$. By Bayes' rule, we obtain the posterior distribution, formally expressed as

$$p(f | \mathcal{D}) \propto \prod_m p(y_m | f, S_m) p(f). \quad (1)$$

To make inference at any arbitrary test point $S_* \in \mathcal{S}$, we marginalise out the latent function to get the posterior belief of our predictive model $g : \mathcal{S} \rightarrow \mathcal{Y}$:

$$p(g(S_*) = y | \mathcal{D}) = \int p(y | f, S_*) p(f | \mathcal{D}) dg. \quad (2)$$

For regression tasks, the likelihood is often assumed to be Gaussian, which provides us with a closed-form expression for both the posterior distribution and the posterior predictive distribution. For classification tasks, the likelihood becomes non-Gaussian. Hence, approximate inference is invoked to form an approximate posterior $q(f) \approx p(f | \mathcal{D})$ in the latent space. Variational GPs [Oppen and Archambeau, 2009] are commonly employed for this purpose, where the variational distribution q (typically a parameterised Gaussian) is learned by maximising the Evidence Lower Bound (ELBO)

$$\text{ELBO} := \mathbb{E}_{f \sim q} \left(\log p(y | f, S) - \text{KL}(q(f) \| p(f)) \right), \quad (3)$$

where $\text{KL}(\cdot \parallel \cdot)$ is the Kullback-Leibler divergence. Additionally, the kernel hyperparameters can be learned by jointly optimising the ELBO alongside the variational parameters, thus not requiring a validation set to tune them.

Although we have described the general framework, we have not yet specified how to leverage the topology or attributes of an SC when predicting its label. The approach we develop in the following sections involves constructing a representation for each SC by applying the *wavelet transform* to its attributes. These representations can then be passed as inputs to a GP.

3 Hodge Laplacian and its Decomposition

We recall from Section 2.1 that a SC is naturally equipped with a sequence of incidence matrices B_k . When acting on a signal over the simplices (i.e. the attribute vectors), these can be interpreted as discrete differential operators. More specifically, B_k and its adjoint B_k^\top are discrete analogues of the divergence and gradient operators [Lim, 2020], respectively. In this section, we present the (discrete) *Hodge Laplacian* and its key decomposition.

3.1 Discrete Hodge Laplacian

In Euclidean spaces, the Laplace operator is the divergence of the gradient of a function, and measures how much the average value of a function around a point differs from the value at the point itself. For graphs, a similar notion is given by the *graph Laplacian*

$$L_0 := B_1 B_1^\top \in \mathbb{Z}^{N_0 \times N_0}, \quad (4)$$

where B_1 is known as the graph incidence matrix. This can be extended to simplicial complexes by considering the Hodge Laplacian [Lim, 2020]

$$L_k := L_k^{\text{low}} + L_k^{\text{up}} \in \mathbb{Z}^{N_k \times N_k}, \quad (5)$$

where $L_k^{\text{low}} := B_k^\top B_k$ is the *lower Laplacian* and $L_k^{\text{up}} := B_{k+1} B_{k+1}^\top$ is the *upper Laplacian*. The lower Laplacian encodes interactions between the k -simplices via the $(k-1)$ -simplices, whereas the upper Laplacian captures interactions between the k -simplices via the $(k+1)$ -simplices.

Note that the Hodge Laplacian is not the only possible choice for a discrete notion of the Laplace operator [Bodnar et al., 2022]. However, it has the particular advantage of being able to define the *Hodge decomposition*, which we discuss next.

3.2 Hodge Decomposition

The *Helmholtz decomposition*, often called the fundamental theorem of vector calculus, states that a vector field can be uniquely decomposed into a sum of three orthogonal vector fields: a *curl-free* field that has no vortices, a *divergence-free* field that has no sources or sinks, and a *harmonic* field that is both curl-free and divergence-free. In turn, the Hodge decomposition adapts this result to simplicial complexes [Lim, 2020], enabling a unique decomposition of the attribute space into the direct sum

$$\mathbb{R}^{N_k} = \text{im}(B_k^\top) \oplus \text{im}(B_{k+1}) \oplus \ker(L_k). \quad (6)$$

The subspaces $\text{im}(B_k^\top)$, $\text{im}(B_{k+1})$ and $\ker(L_k)$ are referred to as the exact, co-exact, and harmonic subspaces, respectively. Together, they are collectively referred to as the *Hodge subspaces*.

The Hodge decomposition implies that the eigendecomposition of the Laplacian $L_k = U_k \Lambda_k U_k^\top$ can be further decomposed according to these Hodge subspaces,

$$U_k = [U_{ke} \ U_{kc} \ U_{kh}] \in \mathbb{R}^{N_k \times (N_{ke} + N_{kc} + N_{kh})}, \quad (7)$$

$$\Lambda_k = \text{diag}(\Lambda_{ke}, \Lambda_{kc}, \Lambda_{kh}) \in \mathbb{R}^{N_k \times (N_{ke} + N_{kc} + N_{kh})}, \quad (8)$$

where (Λ_{ke}, U_{ke}) and (Λ_{kc}, U_{kc}) are the non-zero eigenpairs of the lower and upper Laplacians L_k^{low} and L_k^{up} , respectively, and (Λ_{kh}, U_{kh}) are the zero eigenpairs (i.e. $\Lambda_{kh} = \mathbf{0}$) of the Hodge Laplacian L_k . The strength of this decomposition is that each component can be dealt with separately. For example, the harmonic term contains topological information about the number of k -dimensional

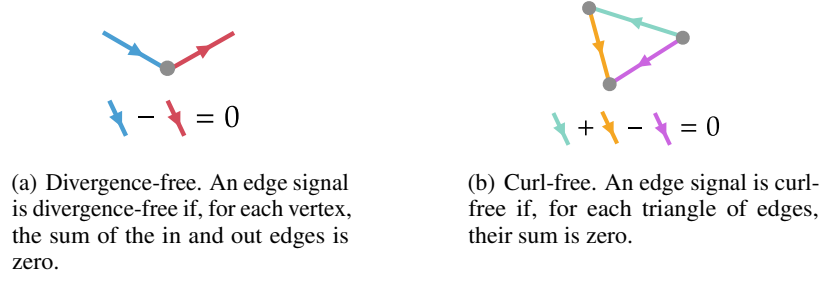


Figure 2: Edge signals in the exact subspace are curl-free, while they are divergence-free in the co-exact subspace. In the harmonic subspace, they are both divergence-free and curl-free.

holes in the SC. Furthermore, a signal can often have a more predominant component (e.g. co-exact) than others. Having a way to control this in the model can help increase the predictive capability.

We observe that when $k = 0$, the lower Laplacian is zero and the exact subspace vanishes. This is explained by the absence of simplices “before” the 0-simplices. Similarly, the upper Laplacian for $k = K + 1$ is zero and the co-exact subspace vanishes. For graphs, this implies that the vertex attributes do not have exact components, and likewise, the edge attributes do not have co-exact components. This reduces the effectiveness of the decomposition. Nevertheless, it is possible to still obtain a co-exact subspace by artificially augmenting the graph with its 3-cliques, thus, converting it into a simplicial 2-complex.

4 Hodgelet Representation for SCGP Predictions

We are now ready to present a representation of attributed SC inputs that exploits both the attributes of the SC and its topology. In Section 3, we saw that the Hodge Laplacian is a discrete differential operator over the attributes that captures the structure (i.e., the interactions between different simplex types) of a SC. As we shall see, the Hodge Laplacian is conveniently related to the notion of *Fourier transforms*.

4.1 Hodgelet Transforms

The Fourier transform of a signal defined on the k -simplices is its projection onto the eigenbases of the Hodge Laplacian L_k . This allows one to manipulate this signal in the spectral domain, making it possible to highlight specific frequencies (which are related to the eigenvalues of the Hodge Laplacian) that are useful for prediction. This can reveal patterns and trends that may not be apparent from examining the original signal. However, the Fourier transform is limited in that it is not localised in space, i.e. not able to capture spatial patterns in the signal.

To overcome this, the wavelet transform can be used, which provides simultaneous localisation in space and frequencies that best adapt to the signals at hand. Fortunately, the classical wavelet transform on \mathbb{R}^n can be adapted to signals on graphs [Hammond et al., 2011] and simplicial complexes [Barbarossa and Sardellitti, 2020]. This is achieved by firstly applying the *wavelet filter* on the eigenvalues of the Hodge Laplacian, defined by

$$w_k(\lambda) := a_k(\alpha_k \lambda) + \sum_{l=1}^{L_k} b_k(\beta_{kl} \lambda), \quad P_k := \{\alpha_k, \beta_{k1}, \dots, \beta_{kL_k}\}. \quad (9)$$

where $a_k : \mathbb{R} \rightarrow \mathbb{R}$ is a *scaling function*, L_k is the number of band-pass scales, $b_k : \mathbb{R} \rightarrow \mathbb{R}$ is a *wavelet function*, and P_k is the wavelet parameter set. The wavelet function acts as a band-pass filter that captures information from medium to high frequencies, and the scaling function serves as a low-pass filter that captures low frequency information. We will apply a wavelet filter to each Hodge component $\Lambda_{ke}, \Lambda_{kc}, \Lambda_{kh}$ individually, instead of applying one on the full eigenvalue set Λ_k , for added flexibility — denote these filters by w_{ke}, w_{kc} , and w_{kh} , with corresponding parameter sets P_{ke}, P_{kc} , and P_{kh} , respectively. Then, the k -simplex wavelet transforms [Barbarossa and Sardellitti,

2020] on each Hodge components are defined as the matrices¹

$$\mathbf{W}_{P_{ke}} := \mathbf{U}_{ke} w_{ke} (\mathbf{\Lambda}_{ke}) \mathbf{U}_{ke}^\top \in \mathbb{R}^{N_{ke} \times N_k}, \quad (10)$$

$$\mathbf{W}_{P_{kc}} := \mathbf{U}_{kc} w_{kc} (\mathbf{\Lambda}_{kc}) \mathbf{U}_{kc}^\top \in \mathbb{R}^{N_{kc} \times N_k}, \quad (11)$$

$$\mathbf{W}_{P_{kh}} := \mathbf{U}_{kh} w_{kh} (\mathbf{\Lambda}_{kh}) \mathbf{U}_{kh}^\top \in \mathbb{R}^{N_{kh} \times N_k}. \quad (12)$$

When applied to the signal (i.e. the attributes), the wavelet transforms yield the *Hodgelet coefficients*

$$\hat{\mathbf{x}}_{ke} := \mathbf{W}_{P_{ke}} \mathbf{x}_k \in \mathbb{R}^{N_{ke}}, \quad \hat{\mathbf{x}}_{kc} := \mathbf{W}_{P_{kc}} \mathbf{x}_k \in \mathbb{R}^{N_{kc}}, \quad \hat{\mathbf{x}}_{kh} := \mathbf{W}_{P_{kh}} \mathbf{x}_k \in \mathbb{R}^{N_{kh}}. \quad (13)$$

These coefficients are sound candidates for an SC representation, as they simultaneously capture information in the attributes as well as the structural information of the SC. However, we do not use these as inputs to our model (e.g. GP) at this stage, since this representation is not invariant under SC isomorphisms. To truly define models with (attributed) graph / SC input, we expect it to be invariant under their isomorphisms [Borgwardt et al., 2020].

4.2 Hodgelet Representations

To this end, we consider pooling the Hodgelet coefficients (13) using an aggregation function, similar to those used in message passing neural networks Gilmer et al. [2017]. Our only restriction on this function is that it must be permutation-invariant (to respect the SC isomorphism) and output a scalar value. As a simple example, we can consider the “energy”, i.e., the squared 2-norm,

$$A_{ke} := \|\hat{\mathbf{x}}_{ke}\|^2, \quad A_{kc} := \|\hat{\mathbf{x}}_{kc}\|^2, \quad A_{kh} := \|\hat{\mathbf{x}}_{kh}\|^2. \quad (14)$$

Due to the commutativity of the sum operation, this is permutation-invariant. We may also explore alternatives, such as the sum, min and max operators, or even a weighted combination of these. This could be useful, for example in settings where the overall parity of the signal is essential for prediction, then we expect the sum to be a more appropriate aggregation function over the norm.

Next, for each $0 \leq k \leq K$, we form the *Hodgelet representations* by concatenating the aggregated coefficients over the wavelet filters $1 \leq f \leq F_k$,

$$\mathbf{r}_{ke} := \begin{bmatrix} A_{ke}^1 & \cdots & A_{ke}^{F_k} \end{bmatrix}^\top \in \mathbb{R}^{F_k}, \quad (15)$$

$$\mathbf{r}_{kc} := \begin{bmatrix} A_{kc}^1 & \cdots & A_{kc}^{F_k} \end{bmatrix}^\top \in \mathbb{R}^{F_k}, \quad (16)$$

$$\mathbf{r}_{kh} := \begin{bmatrix} A_{kh}^1 & \cdots & A_{kh}^{F_k} \end{bmatrix}^\top \in \mathbb{R}^{F_k}. \quad (17)$$

Note that by using multiple wavelet filters instead of a single one, we are able to achieve a more comprehensive representation of the SC signal at multiple resolutions.

Remark 1. In our discussion in Section 2.1, we assumed that $D_k = 1$ (recall that D_k is the dimension of the k -simplices attribute vector). Extending to the case $D_k > 1$ can be achieved by applying the above procedure to each dimension independently and stacking them, resulting in vector-valued aggregations $\mathbf{A}_{ke}^i, \mathbf{A}_{kc}^i, \mathbf{A}_{kh}^i \in \mathbb{R}^{D_k}$ for $1 \leq i \leq F_k$. The corresponding Hodgelet representations then have the dimension $F_k D_k$ instead of F_k .

Remark 2. The most costly procedure in computing Hodgelet coefficients is to obtain the eigendecompositions of \mathbf{L}_k , which scale cubically with respect to the number of k -simplices N_k . For large graphs, we may consider using a polynomial-based approximation, as in [Defferrard et al., 2016]. Nevertheless, we note that the sizes of the SCs involved in prediction tasks are typically small. Hence, this computation is tractable in a wide range of settings, even without using approximations.

¹Here, the wavelet filters $w_{k\bullet}$ are applied component-wise to the eigenvalue matrices $\mathbf{\Lambda}_{k\bullet}$.

4.3 Hodgelet Kernel Function

Given the Hodgelet representations, we can now define kernels of our GP $f : \mathcal{S} \rightarrow \mathbb{R}$. This is defined as either an additive or a product kernel over the simplex dimensions:

$$\kappa_{\text{add}}(S, S') := \sum_{k=1}^K \left(\kappa_{ke}(\mathbf{r}_{ke}, \mathbf{r}'_{ke}) + \kappa_{kc}(\mathbf{r}_{kc}, \mathbf{r}'_{kc}) + \kappa_{kh}(\mathbf{r}_{kh}, \mathbf{r}'_{kh}) \right), \quad (18)$$

$$\kappa_{\text{prod}}(S, S') := \prod_{k=1}^K \left(\kappa_{ke}(\mathbf{r}_{ke}, \mathbf{r}'_{ke}) + \kappa_{kc}(\mathbf{r}_{kc}, \mathbf{r}'_{kc}) + \kappa_{kh}(\mathbf{r}_{kh}, \mathbf{r}'_{kh}) \right), \quad (19)$$

for $S, S' \in \mathcal{S}$, where $\kappa_{ke}, \kappa_{kc}, \kappa_{kh}$ are chosen to be standard kernels over Euclidean space, such as the RBF or the Matérn family of kernels. We choose the inner summand / multiplicand of both (18) and (19) to be additive over the Hodge subspaces to reflect the additive structure of the Hodge decomposition (6). The hyperparameters of the kernels are jointly optimised with the wavelet parameters. We note that, as usual, the training and inference costs scale cubically in the number of SCs, which can be reduced by using inducing points (c.f. Titsias [2009], Hensman et al. [2013]). The eigendecompositions are a one-off cost that can be performed offline.

We highlight that using separate kernels for each Hodge component offers greater modelling flexibility than using a single kernel, leading to improved predictive capability [Yang et al., 2024]. In addition, our construction has the advantage of supporting continuous multi-dimensional simplex attributes, as well as SCs of varying sizes, in contrast to typical graph kernel-based methods. While we only consider the Hodgelet representations as inputs to GPs here, they can trivially be used as inputs to other machine learning methods. However, we note that a major benefit of using GPs over other models is that they allow for easy selection of hyperparameters (i.e. the wavelet parameters and the kernel hyperparameters) via maximum marginal likelihood estimation.

5 Experiments

In this section, we explore three diverse series of experiments involving different predictive tasks, in particular, binary classification, multi-class classification and regression. Our aim is to demonstrate that: (1) adding edge information generally improves the performance of our models, (2) the Hodge decomposition offers a natural way of increasing the flexibility of our SC representations, and (3) when edge attributes are present, it is preferable to treat them as edge attributes rather than as vertex attributes on the corresponding line graph.

For baseline models, we consider commonly used graph neural network (GNN) architectures. This includes the GCN [Kipf and Welling, 2017], GAT [Veličković et al., 2018], GIN [Hu et al., 2020] and the Graph Transformer [Shi et al., 2021] models. It should be noted that GCN uses only vertex attributes, while GAT, GIN, and Transformer use both vertex and edge attributes. We distinguish between GP models that use SC representations based on the wavelet transform or the Hodgelet transforms, which we denote by WTGP and HTGP, respectively. The latter applies wavelet transforms to each Hodge component separately, while the former does not split signals into their Hodge components. We also use the indices “vertex”, “edge” or “hybrid” to indicate whether we use only vertex attributes, edge attributes, or both vertex and edge attributes for our prediction. Hence, for example, the model “WTGP (vertex)”, uses a SC representation based on the wavelet transform over only the vertex attributes. This is identical to the GP model in Opolka et al. [2023].

Lastly, we note that all experiments are conducted on Nvidia P100 GPUs, and all models are evaluated on each dataset using 5-fold cross-validation. Details of all experiments can be found in Appendix B.

5.1 Vector field classification

We first conduct experiments on two synthetic datasets, which we refer to as Div-curl-free and Vortices. Both contain 100 graphs that represent discretisations of noisy vector fields via the *de Rham map* [Desbrun et al., 2008], which transforms vector fields into attributed simplicial 2-complexes with signals on the edges (see Appendix B.2). In Div-curl-free, the task is to determine whether a given vector field is predominantly divergence-free or curl-free; for Vortices, the task is to determine whether the net circulation of a vortex-dominated fluid flow is positive or negative (i.e., anticlockwise

or clockwise). Each task is performed on different mesh resolutions, given by the number of vertices, ranging from 10 to 150. We also construct line graph counterparts on which WTGP (vertex) and HTGP (vertex) are executed. The goal of this experiment is to show that (1) operating directly with edge attributes is more effective than working with vertex attributes on the corresponding line graphs, and (2) the flexibility offered by the Hodge decomposition improves the model accuracy.

In Figure 3, we display the results on both datasets, where we compared the accuracy of the GP models at different mesh resolutions. On both experiments, we firstly observe a sharp performance drop when converting edge-attributed graphs into line graphs with vertex attributes, highlighting the importance of preserving edge-level structure. A likely reason is that the notion of “directionality”, present in edges is lost when converting to line graphs. Secondly, we find that HTGP (edge) is the best-performing model on both experiments and is surprisingly robust to the mesh resolution. For Div-curl-free, it is reasonable to assume that the other models do not perform well, since they have no means to distinguish the curl-free (exact) part from the divergence-free (co-exact) part. However, on coarse meshes consisting of only 10 or 25 vertices, the discretised curl / divergence-free vector fields are far from exact / co-exact, making the classification task challenging. Despite this, HTGP (edge) is able to pick up signals to predict labels correctly. For Vortices, the prediction task does not require explicit knowledge of the Hodge decomposition; thus, we see that the performance of WTGP (edge) without the Hodge decomposition continually improves with increasing resolution. However, the result of HTGP (edge) performs well in all resolutions. We believe that this is because flows generated by the vortices are divergence-free. Hence, the flexibility given by the Hodge decomposition allows the model to focus on the co-exact component, while downplaying unnecessary contributions from the exact and harmonic components, leading to increased robustness.

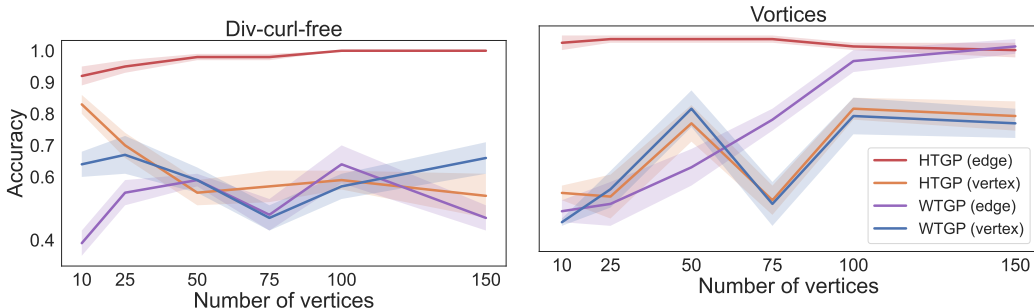


Figure 3: Comparison of the WTGP/HTGP models on the vector field classification benchmarks. We consider ablation in mesh resolution. Shaded regions indicate standard error from the mean accuracy.

5.2 TUDataset and MoleculeNet

This second series of datasets are taken from the standard biological graph benchmarks TUDataset [Morris et al., 2020] and MoleculeNet [Wu et al., 2017]. The vertex attributes of these datasets are generally a mix of scalars (e.g. atom charge, atom coordinates) and categories (e.g. atom type). The edge attributes are always categorical (e.g. bond type). Out of the benchmarks we consider, MUTAG and AIDS are binary classification tasks, while FreeSolv and ESOL are regression tasks. Our goal here is to apply our method to real-world datasets and show that adding edge information and using Hodge decomposition can improve the overall performance. We summarise our results in Table 1.

For MUTAG, we observe that HTGP (hybrid), WTGP (hybrid) and HTGP (edges) are the top three best-performing models, respectively, surpassing the GNN baselines. The benefit of using information from both the vertex and edge attributes is clear, with models that include the edge attributes generally outperforming the same model that uses only the vertex attributes. We also observe that the HTGP models perform better than the corresponding WTGP models, suggesting that the flexibility afforded by the Hodge decomposition contributes to improved performance. For AIDS, we see that although the GAT and GIN baselines are the best-performing, the results of WTGP (edge), WTGP (hybrid) and HTGP (edge) are similarly high. On this data, we see that incorporating edge information is crucial for competitive performance. For FreeSolv and ESOL, we find that HTGP (hybrid), WTGP (hybrid), HTGP (vertex), and WTGP (vertex) all outperform the GNN baselines, highlighting the strength of the GP models on regression tasks. Experiments on the edge-only models suggest that

	Accuracy (\uparrow)		Mean squared error (\downarrow)	
	MUTAG	AIDS	FreeSolv	ESOL
GCN (vertex)	0.660 ± 0.008	0.985 ± 0.004	9.20 ± 0.64	1.64 ± 0.12
GAT (hybrid)	0.740 ± 0.022	0.996 ± 0.002	3.42 ± 0.34	1.15 ± 0.08
GIN (hybrid)	0.830 ± 0.033	0.996 ± 0.001	2.81 ± 0.17	1.17 ± 0.15
Transformer (hybrid)	0.718 ± 0.040	0.984 ± 0.002	2.18 ± 0.12	0.75 ± 0.10
WTGP (hybrid)	0.851 ± 0.018	0.994 ± 0.001	1.52 ± 0.08	0.72 ± 0.06
WTGP (vertex)	0.813 ± 0.023	0.992 ± 0.002	1.87 ± 0.63	0.50 ± 0.01
WTGP (edge)	0.824 ± 0.023	0.995 ± 0.002	13.84 ± 2.27	2.05 ± 0.07
HTGP (hybrid)	0.872 ± 0.019	0.992 ± 0.002	1.49 ± 0.17	0.51 ± 0.02
HTGP (vertex)	0.840 ± 0.020	0.993 ± 0.003	1.39 ± 0.13	0.50 ± 0.02
HTGP (edge)	0.850 ± 0.024	0.994 ± 0.002	11.05 ± 1.53	1.54 ± 0.06

Table 1: We display the mean and standard error of results across five random seeds. Colours indicate the **best**, **second-best**, and **third-best** result for each dataset.

on these datasets, the edge information is detrimental to performance. However, using both edge and vertex attributes in WTGP (hybrid) and HTGP (hybrid), the negative contribution from edges is compensated, owing to the flexibility of our kernel design. As with MUTAG, our best-performing models are those that use the Hodgelet representations.

In total, our models (in particular the HTGP) are always among the top performers, demonstrating their versatility and broad applicability.

5.3 PowerGraph

In the last series of experiments, we consider prediction tasks in electricity networks using the ieee24 data from the PowerGraph benchmark [Varbella et al., 2024]. This real-world dataset has been downsampled to fit the setting of a small data regime (see Appendix B.1). The graphs in ieee24 represent power grids at different pre-outage operating conditions. Here, the vertices represents electrical buses, whereas the edges correspond to transmission lines and transformers. The attributes on the vertices consist of active power generation, reactive power generation, active power demand, reactive power demand, voltage magnitude, voltage angle, the number of loads, and the number of generators. The edge attributes consist of branch conductance and branch susceptance. The benchmark consists of three tasks: binary classification, multi-class classification and regression. These involve determining whether (binary classification) and to what extent (multiclass classification and regression) a power grid is stable or not. In our results, displayed in Table 2, we observe that on all three tasks, HTGP (hybrid) and HTGP (edge) have the best and second-best performance, respectively. The performance of these two models is superior to that of the GNN baselines. We observe that incorporating edge information and Hodge decomposition clearly improves performance across all tasks.

6 Conclusion

In this paper, we propose a method for creating a representation for attributed SCs and graphs that enables prediction tasks on SCs and graphs. This approach can be easily combined with GPs to create a robust and interpretable method that achieves competitive performance across a variety of datasets. The key contribution lies in the fact that our Hodgelet representations leverage both the wavelet transform of attributes and the Hodge decomposition. The wavelet transform captures multi-scale spectral and spatial information, while the Hodge decomposition enables finer control by separating the signal into exact, co-exact and harmonic components. In terms of possible future directions, we first intend to incorporate the geometry of the SC, e.g. the curvature [Ni et al., 2019], which has been shown to be useful for molecular prediction tasks [Fang et al., 2022], and secondly to adapt our approach to prediction tasks at the level of vertices or edges. In this work, we have been able to advance the state-of-the-art by developing a general framework that can tackle a diverse range of tasks. This unlocks the potential for GPs to be used in a variety of graph and SC-level problems.

	Accuracy (\uparrow)		Mean squared error (\downarrow)
	ieee24-binary	ieee24-multiclass	ieee24-regression ($\times 10^{-4}$)
GCN (vertex)	0.689 ± 0.010	0.538 ± 0.028	6.23 ± 3.36
GAT (hybrid)	0.776 ± 0.008	0.528 ± 0.028	7.20 ± 4.15
GIN (hybrid)	0.861 ± 0.017	0.760 ± 0.025	5.12 ± 3.83
Transformer (hybrid)	0.842 ± 0.011	0.734 ± 0.068	1.83 ± 0.72
WTGP (hybrid)	0.834 ± 0.012	0.866 ± 0.019	3.20 ± 0.39
WTGP (vertex)	0.785 ± 0.012	0.848 ± 0.011	3.80 ± 0.58
WTGP (edge)	0.838 ± 0.020	0.826 ± 0.019	5.28 ± 1.94
HTGP (hybrid)	0.940 ± 0.004	0.948 ± 0.012	1.29 ± 0.09
HTGP (vertex)	0.831 ± 0.025	0.880 ± 0.019	2.08 ± 0.13
HTGP (edge)	0.929 ± 0.005	0.928 ± 0.014	1.68 ± 0.12

Table 2: We display the mean and standard error of results across five random seeds. Colours indicate the **best**, **second-best**, and **third-best** result for each dataset.

Acknowledgments

MA is supported by a Mathematical Sciences Doctoral Training Partnership held by Prof. Helen Wilson, funded by the Engineering and Physical Sciences Research Council (EPSRC), under Project Reference EP/W523835/1. ST is supported by a Department of Defense Vannevar Bush Faculty Fellowship held by Prof. Andrew Stuart, and by the SciAI Center, funded by the Office of Naval Research (ONR), under Grant Number N00014-23-1-2729.

References

- Mathieu Alain, So Takao, Brooks Paige, and Marc P Deisenroth. Gaussian processes on cellular complexes. In *International Conference on Machine Learning*, 2024a. (cited on pages 2 and 13)
- Mathieu Alain, So Takao, Bastian Rieck, Xiaowen Dong, and Emmanuel Noutahi. Graph Classification Gaussian Processes via Hodgelet Spectral Features. In *Advances in Neural Information Processing Systems (NeurIPS) 2024 Workshop Workshop on Bayesian Decision-making and Uncertainty (BDU)*, 2024b. URL <https://arxiv.org/pdf/2410.10546>. (cited on page 2)
- Federica Baccini, Filippo Geraci, and Ginestra Bianconi. Weighted simplicial complexes and their representation power of higher-order network data and topology. *Physical Review E*, 2022. (cited on page 13)
- Rubén Ballester, Ernst Röell, Daniel Bin Schmid, Mathieu Alain, Sergio Escalera, Carles Casacuberta, and Bastian Rieck. Mantra: The manifold triangulations assemblage. *arXiv preprint arXiv:2410.02392*, 2024. (cited on page 1)
- Sergio Barbarossa and Stefania Sardellitti. Topological signal processing over simplicial complexes. *IEEE Transactions on Signal Processing*, 2020. (cited on pages 2 and 5)
- Claudio Battiloro, Paolo Di Lorenzo, and Sergio Barbarossa. Topological slepians: Maximally localized representations of signals over simplicial complexes. In *IEEE International Conference on Acoustics, Speech and Signal Processing*, 2023. (cited on page 2)
- J Thomas Beale and Andrew Majda. High order accurate vortex methods with explicit velocity kernels. *Journal of Computational Physics*, 58(2):188–208, 1985. (cited on page 16)
- Cristian Bodnar, Francesco Di Giovanni, Benjamin Chamberlain, Pietro Lió, and Michael Bronstein. Neural sheaf diffusion: A topological perspective on heterophily and oversmoothing in gnns. In *Advances in Neural Information Processing Systems*, 2022. (cited on page 4)
- Karsten Borgwardt, Elisabetta Ghisu, Felipe Llinares-López, Leslie O’Bray, and Bastian Rieck. Graph kernels: State-of-the-art and future challenges. *Foundations and Trends in Machine Learning*, 2020. (cited on pages 1 and 6)

- Michael Bronstein, Joan Bruna, Taco Cohen, and Petar Veličković. *Geometric Deep Learning Grids, Groups, Graphs, Geodesics, and Gauges*. arXiv, 2021. (cited on page 1)
- Michaël Defferrard, Xavier Bresson, and Pierre Vandergheynst. Convolutional neural networks on graphs with fast localized spectral filtering. In *Conference on Neural Information Processing Systems*, 2016. (cited on page 6)
- Mathieu Desbrun, Eva Kanso, and Yiyong Tong. *Discrete Differential Forms for Computational Modeling*, pages 287–324. Birkhäuser Basel, 2008. (cited on pages 7 and 14)
- Xiaomin Fang, Lihang Liu, Jieqiong Lei, Donglong He, Shanzhuo Zhang, Jingbo Zhou, Fan Wang, Hua Wu, and Haifeng Wang. Geometry-enhanced molecular representation learning for property prediction. *Nature Machine Intelligence*, 4(2):127–134, 2022. (cited on page 9)
- Yifan Feng, Haoxuan You, Zizhao Zhang, Rongrong Ji, and Yue Gao. Hypergraph neural networks. In *AAAI Conference on Artificial Intelligence*, 2019. (cited on page 13)
- Matthias Fey and Jan E. Lenssen. Fast graph representation learning with PyTorch Geometric. In *ICLR Workshop on Representation Learning on Graphs and Manifolds*, 2019. (cited on page 14)
- Jacob Gardner, Geoff Pleiss, Kilian Q Weinberger, David Bindel, and Andrew G Wilson. Gpytorch: Blackbox matrix-matrix gaussian process inference with gpu acceleration. In *Advances in Neural Information Processing Systems*, 2018. (cited on page 14)
- Justin Gilmer, Samuel S Schoenholz, Patrick F Riley, Oriol Vinyals, and George E Dahl. Neural message passing for quantum chemistry. In *International conference on machine learning*, pages 1263–1272. PMLR, 2017. (cited on page 6)
- David K Hammond, Pierre Vandergheynst, and Rémi Gribonval. Wavelets on graphs via spectral graph theory. *Applied and Computational Harmonic Analysis*, 2011. (cited on pages 2 and 5)
- James Hensman, Nicolo Fusi, and Neil D Lawrence. Gaussian processes for big data. *arXiv preprint arXiv:1309.6835*, 2013. (cited on page 7)
- Weihua Hu, Bowen Liu, Joseph Gomes, Marinka Zitnik, Percy Liang, Vijay Pande, and Jure Leskovec. Strategies for Pre-training Graph Neural Networks. In *International Conference on Learning Representations*, 2020. (cited on page 7)
- Elvin Isufi, Geert Leus, Baltasar Beferull-Lozano, Sergio Barbarossa, and Paolo Di Lorenzo. Topological signal processing and learning: Recent advances and future challenges. *Signal Processing*, 2025. (cited on page 2)
- Thomas Kipf and Max Welling. Semi-supervised Classification with Graph Convolutional Networks. In *International Conference on Learning Representations*, 2017. (cited on page 7)
- Lek-Heng Lim. Hodge laplacians on graphs. *SIAM Review*, 2020. (cited on page 4)
- Dongsheng Luo, Wei Cheng, Dongkuan Xu, Wenchao Yu, Bo Zong, Haifeng Chen, and Xiang Zhang. Parameterized explainer for graph neural network. *Advances in neural information processing systems*, 2020. (cited on page 1)
- Christopher Morris, Nils M. Kriege, Franka Bause, Kristian Kersting, Petra Mutzel, and Marion Neumann. Tudataset: A collection of benchmark datasets for learning with graphs. In *ICML 2020 Workshop on Graph Representation Learning and Beyond*, 2020. (cited on page 8)
- Paul K Newton. N-vortex problem: Analytical techniques. *Appl. Mech. Rev.*, 55(1):B15–B16, 2002. (cited on page 16)
- Chien-Chun Ni, Yu-Yao Lin, Feng Luo, and Jie Gao. Community detection on networks with ricci flow. *Scientific Reports volume*, 2019. (cited on page 9)
- Felix Opolka, Yin-Cong Zhi, Pietro Liò, and Xiaowen Dong. Graph classification gaussian processes via spectral features. In *Conference on Uncertainty in Artificial Intelligence*, 2023. (cited on pages 2 and 7)

- Manfred Opper and Cédric Archambeau. The variational gaussian approximation revisited. *Neural Computation*, 2009. (cited on page 3)
- Antonio Ortega, Pascal Frossard, Jelena Kovacëvić, José MF Moura, and Pierre Vandergheynst. Graph signal processing: Overview, challenges, and applications. *Proceedings of the IEEE*, 2018. (cited on page 2)
- Theodore Papamarkou, Tolga Birdal, Michael Bronstein, Gunnar Carlsson, Justin Curry, Yue Gao, Mustafa Hajj, Roland Kwitt, Pietro Liò, Paolo Di Lorenzo, Vasileios Maroulas, Nina Miolane, Farzana Nasrin, Karthikeyan Natesan Ramamurthy, Bastian Rieck, Simone Scardapane, Michael T Schaub, Petar Veličković, Bei Wang, Yusu Wang, Guo-Wei Wei, and Ghada Zamzmi. Position: Topological deep learning is the new frontier for relational learning. In *International Conference on Machine Learning*, 2024. (cited on pages 1 and 13)
- Adam Paszke, Sam Gross, Francisco Massa, Adam Lerer, James Bradbury, Gregory Chanan, Trevor Killeen, Zeming Lin, Natalia Gimelshein, Luca Antiga, Alban Desmaison, Andreas Kopf, Edward Yang, Zachary DeVito, Martin Raison, Alykhan Tejani, Sasank Chilamkurthy, Benoit Steiner, Lu Fang, Junjie Bai, and Soumith Chintala. Pytorch: An imperative style, high-performance deep learning library. In *Advances in Neural Information Processing Systems*, 2019. (cited on page 14)
- Thomas Pinder, Kathryn Turnbull, Christopher Nemeth, and David Leslie. Gaussian processes on hypergraphs. *arXiv preprint arXiv:2106.01982*, 2021. (cited on page 13)
- Ali Rahimi and Benjamin Recht. Random features for large-scale kernel machines. *Advances in neural information processing systems*, 20, 2007. (cited on page 15)
- Carl Edward Rasmussen and Christopher K I Williams. *Gaussian processes for machine learning*. MIT Press, 2005. (cited on pages 1 and 3)
- T Mitchell Roddenberry, Florian Frantzen, Michael T Schaub, and Segarra Santiago. Hodgelets: Localized spectral representations of flows on simplicial complexes. In *International Conference on Acoustics, Speech, and Signal Processing*, 2022. (cited on page 13)
- Yunsheng Shi, Zhengjie Huang, Shikun Feng, Hui Zhong, Wenjing Wang, and Yu Sun. Masked Label Prediction: Unified Message Passing Model for Semi-Supervised Classification. In *International Joint Conference on Artificial Intelligence*, 2021. (cited on page 7)
- Michalis Titsias. Variational learning of inducing variables in sparse gaussian processes. *International Conference on Artificial intelligence and Statistics*, 2009. (cited on page 7)
- Anna Varbella, Kenza Amara, Blazhe Gjorgiev, Mennatallah El-Assady, and Giovanni Sansavini. Powergraph: A power grid benchmark dataset for graph neural networks. In *NeurIPS2024 Track on Datasets and Benchmarks*, 2024. (cited on page 9)
- Petar Veličković, Guillem Cucurull, Arantxa Casanova, Adriana Romero, Pietro Liò, and Yoshua Bengio. Graph Attention Networks. In *International Conference on Learning Representations*, 2018. (cited on page 7)
- Zhenqin Wu, Bharath Ramsundar, Evan N. Feinberg, Joseph Gomes, Caleb Geniesse, Aneesh S. Pappu, Karl Leswing, and Vijay Pande. Moleculenet: A benchmark for molecular machine learning. *arXiv preprint, arXiv: 1703.00564*, 2017. (cited on page 8)
- Maosheng Yang, Viacheslav Borovitskiy, and Elvin Isufi. Hodge-compositional edge gaussian processes. In *International Conference on Artificial Intelligence and Statistics*, 2024. (cited on pages 2, 7, and 13)
- Zhitao Ying, Dylan Bourgeois, Jiaxuan You, Marinka Zitnik, and Jure Leskovec. Gnnexplainer: Generating explanations for graph neural networks. *Advances in neural information processing systems*, 32, 2019. (cited on page 1)
- Hao Yuan, Haiyang Yu, Jie Wang, Kang Li, and Shuiwang Ji. On explainability of graph neural networks via subgraph explorations. In *International conference on machine learning*, 2021. (cited on page 1)

A Simplicial complexes

In this appendix, we provide details on simplicial complexes, which are key objects in our present work. First, we introduce graphs briefly. Graphs are objects consisting of a set of vertices V and edges E , equipped with a map $\phi : E \rightarrow \{\{v_1, v_2\} \mid \forall v_1, v_2 \in V\}$ that identifies each edge $e \in E$ with a pair of vertices $\{v_1, v_2\}$. We may sometimes abuse the notation and simply write $e = \{v_1, v_2\}$. Graph data can support signals on their vertices and edges, resulting in a structure that is richer than tabular data. Common examples are social networks, electrical grids (see Section 5.3), citation networks, traffic maps, collaboration networks, chemical reaction networks, vector fields (see Section 5.1), and molecules (see Section 5.2). However, a limitation of graphs is that they can only encode *dyadic interactions* between vertices through its edges. Multiple recent works have sought to overcome this limitation by using more general structures, such as simplicial complexes, cellular complexes, and hypergraphs [Feng et al., 2019, Baccini et al., 2022, Roddenberry et al., 2022, Alain et al., 2024a, Yang et al., 2024, Papamarkou et al., 2024].

Simplicial complexes. A natural extension of graphs is *simplicial complexes*, which are built from general structures known as *k-simplices*. Abstractly, a *k-simplex* may be understood as a tuple of $k + 1$ vertices. Thus, vertices themselves are 0-simplices, and edges are 1-simplices. Following this, a 2-simplex is just a triangular face (also simply called triangle) formed by three adjacent vertices. This can be used to describe a *triadic interaction* between vertices, i.e., a relation between three vertices.

A *face* of a *k-simplex* is a $k - 1$ -simplex formed by an order k subset of the original set of vertices defining the *k-simplex*. Then, we can define a *simplicial K-complex* \mathcal{K} as a set of *k-simplices* for $k = 0, \dots, K$ such that it satisfies the property that, for every simplex $s \in \mathcal{K}$, its faces are also in \mathcal{K} . In other words, it is a set of sets of order at most K that is closed under the operation of taking non-empty subsets, that is, for $\{v_1, \dots, v_k\} \in \mathcal{K}$, any non-empty subset of $\{v_1, \dots, v_k\}$ is also contained in \mathcal{K} . Thus, for example, a graph $G = (V, E)$ may be understood as a simplicial 1-complex $\mathcal{K} := V \cup E$ since for every $\{v_1, v_2\} \in E \subset \mathcal{K}$, we have that $\{v_i\} \in V \subset \mathcal{K}$ for $i = 1, 2$.

In this work, we will primarily be concerned with simplicial 2-complexes, which consist of vertices, edges and triangular faces. We denote this by a triple (V, E, T) , where V is the vertex set, E is the edge set, and T is the triangle set. By our definition above, this tuple is required to satisfy the following closure conditions:

1. all vertices that form an edge in E must be in V ,
2. all edges that form a triangle in T must be in E .

We further impose that there cannot be self-edges (self-loops) or multi-edges. Finally, the number of vertices, edges, and triangles in V, E and T will be denoted by N_v, N_e and N_t , respectively.

Orientation. Here, we give a notion of *orientation* to a simplicial complex \mathcal{K} . Simply, an orientation on a simplicial complex refers to a choice of ordering of elements in $\{v_1, \dots, v_k\}$ for each $\{v_1, \dots, v_k\} \in \mathcal{K}$. More precisely, it is a map sending $\{v_1, \dots, v_k\}$ to an equivalence class of tuples $(v_{\sigma(1)}, \dots, v_{\sigma(k)})$ for some permutation $\sigma \in S_k$, where the equivalence relation is defined by the parity ± 1 of the permutation σ . For an edge $e = \{v_1, v_2\}$, an orientation therefore means the assignment of a direction (v_1, v_2) or (v_2, v_1) . For a triangle $t = \{v_1, v_2, v_3\}$, its orientation is a choice of one of

$$[(v_1, v_2, v_3)] = \{(v_1, v_2, v_3), (v_2, v_3, v_1), (v_3, v_1, v_2)\}, \quad (20)$$

$$[(v_3, v_2, v_1)] = \{(v_3, v_2, v_1), (v_2, v_1, v_3), (v_1, v_3, v_2)\}, \quad (21)$$

which, at an intuitive level, corresponds to orientations that are either clockwise or anticlockwise. We highlight that although an orientation is necessary to express concepts such as edge flows and to define the Laplacian, the choice of orientation itself is arbitrary.

Cellular complexes and hypergraphs. We can further generalise simplicial complexes, by considering the more general structure of *cellular complexes*. The treatment of cellular complexes is similar to that of simplicial complexes; most constructions on simplicial complexes can be extended to the cellular complex setting straightforwardly. For more details, see Alain et al. [2024a]. We can also easily handle hypergraphs (i.e., a structure in which an edge can join any number of vertices) by using Laplacians specialised for hypergraphs [Pinder et al., 2021].

B Experimental details

In this section, we provide additional details regarding the experiments described in Section 5. We recall that the models are evaluated on each dataset using 5-fold cross-validation.

We use PyTorch [Paszke et al., 2019] to implement our algorithm. In particular, we use GPytorch [Gardner et al., 2018] for training Gaussian processes and PyGeometric [Fey and Lenssen, 2019] to process graph data.

B.1 Preprocessing

When applicable, the datasets in Section 5 have been preprocessed to remove disconnected graphs. Furthermore, in cases where no vertex (or edge) attributes were available, a one-hot encoding of the vertex (or edge) degrees was used. Finally, as mentioned in Section 5.3, the datasets ieee24-binary, ieee24-multiclass and ieee24-regression have been downsampled from 21500 graphs to 284, 350 and 125, respectively. For the first two datasets, downsampling was carried out in such a way that there is no class imbalance.

B.2 Vector field classification experiments

Here, we give more details about the vector field classification experiments (Div-curl-free and Vortices) from Section 5.1.

B.2.1 Discretising vector fields via the de Rham map

To project a vector field $\mathbf{X} : \mathbb{R}^2 \rightarrow \mathbb{R}^2$ onto a simplicial 2-complex, we employ the *de Rham map* Desbrun et al. [2008], which “discretises” a vector field into edge signals. For a given oriented edge $e = (v_0, v_1)$ with endpoint coordinates \mathbf{x}_0 and \mathbf{x}_1 , we define the projection X^e of \mathbf{X} onto e by the following integral,

$$X^e := \int_0^1 \mathbf{X}(\mathbf{x}_0 + t(\mathbf{x}_1 - \mathbf{x}_0)) \cdot \hat{\mathbf{t}} dt, \quad (22)$$

where $\hat{\mathbf{t}} := \frac{\mathbf{x}_1 - \mathbf{x}_0}{\|\mathbf{x}_1 - \mathbf{x}_0\|}$ is the unit tangent vector along the edge. Numerically, this can be computed efficiently using numerical quadratures, owing to the fact that the integral is only defined over the 1D interval $[0, 1]$. Note that this depends on the ordering of the vertices v_0 and v_1 characterising the edge – if we flip the order, then the sign of X^e flips. Thus, we require the graph to be oriented in order for the projections $\{X^e\}_{e \in E}$ to be well-defined. In Figure 4, we display an example of such a projection onto a regular triangular mesh.

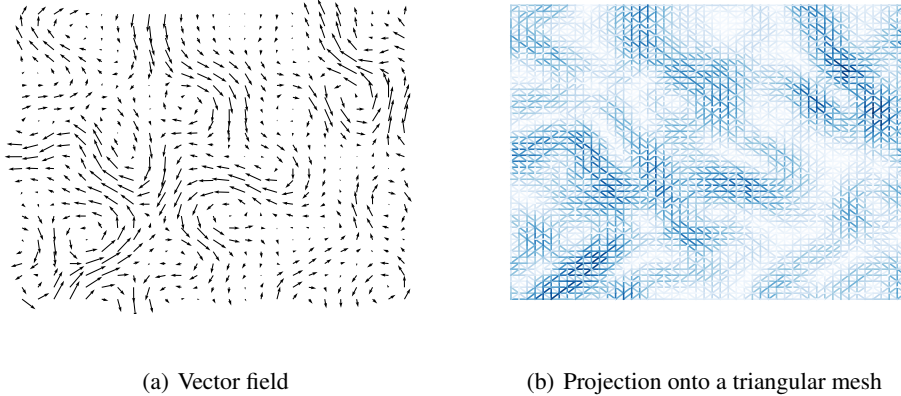


Figure 4: Projection of a continuous vector field onto a regular triangular mesh by applying the de Rham map.

B.2.2 Div-curl-free

In order to generate a random vector field, we first sample a Gaussian process $f : \Omega \times \mathbb{R}^2 \rightarrow \mathbb{R}$, and then take its derivatives f_x, f_y in both spatial components. Noting that a curl-free 2D vector field is always the gradient of a potential, we can sample an arbitrary curl-free field by taking

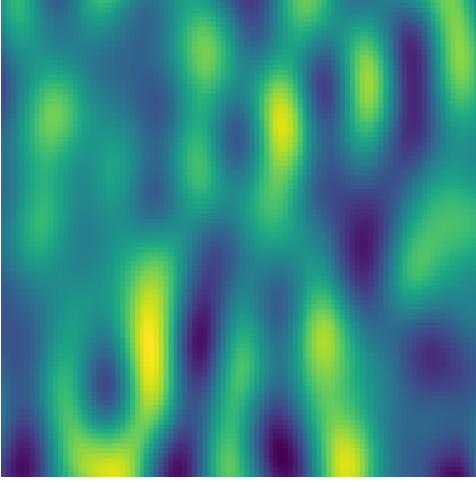
$$\mathbf{X}_{\text{curl-free}} := \nabla f = [f_x, f_y]^\top. \quad (23)$$

Similarly, since a divergence-free 2D vector field is always a *Hamiltonian vector field*, we can choose

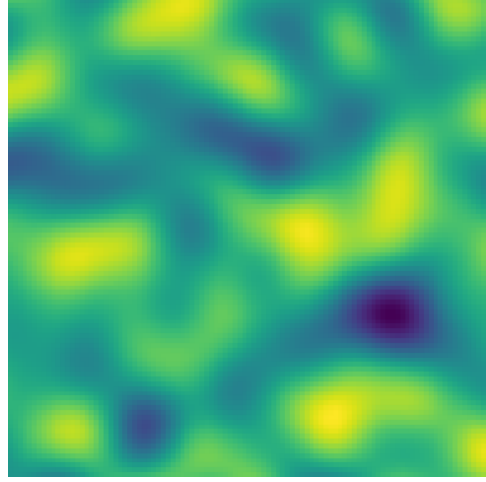
$$\mathbf{X}_{\text{div-free}} := \nabla^\perp f = [f_y, -f_x]^\top, \quad (24)$$

in order to sample an arbitrary divergence-free field.

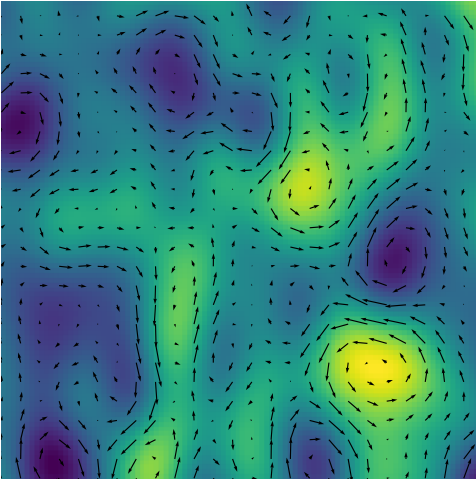
For the scalar field f , we used samples of the squared-exponential Gaussian process, sampled using its random feature approximation Rahimi and Recht [2007]. We display this in Figure 5, where we plot the derivatives f_x, f_y , and their combinations to yield divergence-free and curl-free fields.



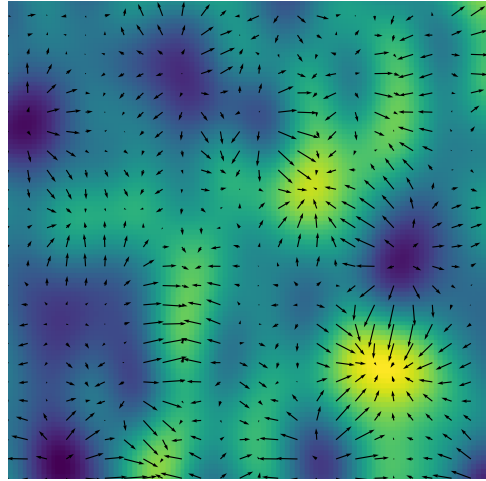
(a) Horizontal gradient f_x of a GP sample



(b) Vertical gradient f_y of a GP sample



(c) Divergence-free field $(f_y, -f_x)$



(d) Curl-free field (f_x, f_y)

Figure 5: Illustration of the random vector field data generating process.

Our data consist of mostly divergence-free and curl-free vector fields, which are generated by considering the linear combination

$$\mathbf{X} := \lambda \mathbf{X}_{\text{div-free}} + (1 - \lambda) \mathbf{X}_{\text{curl-free}} + R\epsilon, \quad (25)$$

where $\lambda \sim U([0.1, 0.9])$, $R > 0$ is the noise level, $\epsilon \sim \mathcal{N}(0, 1)$, and $\mathbf{X}_{\text{div-free}}, \mathbf{X}_{\text{curl-free}}$ generated randomly. If $\lambda < 0.5$, we say that the vector field \mathbf{X} is mostly curl-free, and if $\lambda > 0.5$, we say that it is mostly divergence-free.

B.2.3 Vortices

We generate synthetic vortex-dominated flows by considering the point vortex approximation to fluid flows [Newton, 2002]. This is given by N point vortices with strengths $\Gamma_1, \dots, \Gamma_N$ and locations $\mathbf{x}_1, \dots, \mathbf{x}_N$. To prevent singular velocities occurring at the point vortex locations, we employ vortex blob regularisation [Beale and Majda, 1985] to model the vortex field with a smoothing parameter $\delta = 0.1$. This results in the *streamfunction*

$$\psi_\delta(\mathbf{x}) = - \sum_{n=1}^N \frac{\Gamma_n}{4\pi} [\log(\|\mathbf{x} - \mathbf{x}_n\|^2) - \text{Ei}(-\|\mathbf{x} - \mathbf{x}_n\|^2/\delta^2)], \quad (26)$$

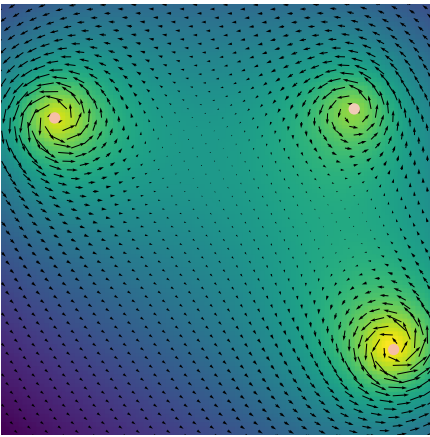
where $\text{Ei}(\cdot)$ denotes the exponential integral, and the corresponding velocity vector field is computed as

$$u(\mathbf{x}) = \frac{\partial \psi_\delta}{\partial y}(\mathbf{x}), \quad v(\mathbf{x}) = -\frac{\partial \psi_\delta}{\partial x}(\mathbf{x}). \quad (27)$$

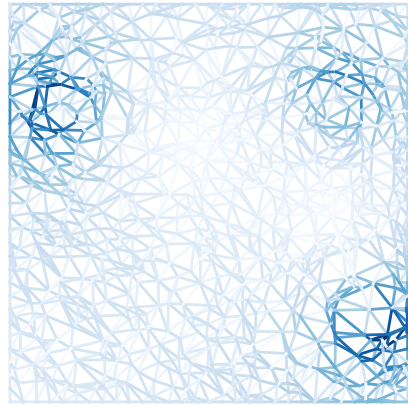
The net circulation Γ of the flow is given approximately by (exact if $\delta = 0$)

$$\Gamma \approx \sum_{n=1}^N \Gamma_n. \quad (28)$$

In our experiments, we set $N = 3$ and generate random vortex-dominated fields by randomly sampling vortex locations i.i.d. uniformly on a $[0, 1] \times [0, 1]$ grid and vortex strengths from i.i.d. standard Gaussians. However, for our experiments, we could not achieve good results when vortex locations were randomly sampled for every data point. Hence, we used fixed locations for all data samples, only making the vortex strengths random. Our final dataset consists of 100 attributed SCs obtained by applying the de Rham map of the resulting vector fields to randomly generated triangular meshes (Figure 6). The corresponding labels are computed using (28) where we use the label “0” for $\Gamma < 0$ and “1” for $\Gamma > 0$.



(a) Fluid flow with 3 vortices



(b) Projection onto a triangular mesh

Figure 6: Projection of a 3-vortex flow onto a randomly generated triangular mesh.

B.3 Model configurations

In Table 3 and 4, we record the hyperparameters used for the GNN baselines on each dataset. These were selected using grid search on the validation set. For our Gaussian process models, we employ the radial basis function (RBF) kernel throughout. For the Hodgelet representations, we use three filters, with their initial values between 4 and 6, and three band-pass scales, initialised with values between 0.1 and 5.0.

The aggregation function is dataset dependent and we choose the best between the energy, the sum and a weighted combination of the sum, min and max operators. In particular, for Div-curl-free, we use the energy (squared 2-norm), and for Vortices, we choose the sum, since the task requires the model to know the overall parity of the circulation (i.e., anticlockwise or clockwise) — the 2-norm does not contain this information, hence using this for Vortices will lead to poor performance.

To optimise the variational evidence lower bound (ELBO), we introduce a scaling constant β between 0.01 and 1, that balances between the expected log-likelihood term and the Kullback–Leibler (KL) regularisation term. Probabilistically, this corresponds to making approximate inference with the prior $p(x)^\beta$. When $\beta < 1$, it reduces the regularising effect coming from the prior. We choose the best values from $\beta \in \{0.01, 0.1, 1.0\}$. For training, we use the AdamW optimiser throughout.

	MUTAG	AIDS	FreeSolv	ESOL
Hidden dim.	128	128	64	32
Num. layers	5	5	3	5
Dropout	0.5	0.5	0	0
Weight decay	5e-5	5e-5	5e-5	5e-5
Aggregation	Sum	Sum	Mean	Sum
Learning rate	0.01	0.01	0.01	0.01
Num. epochs	200	200	300	200
Task	Binary	Binary	Regression	Regression

Table 3: Configurations used for the graph neural network baselines in Table 1.

	ieee24-bin	ieee24-multiclass	ieee24-regression
Hidden dim.	32	32	32
Num. layers	3	3	3
Dropout	0	0	0
Weight decay	5e-5	5e-5	5e-5
Aggregation	Sum	Sum	Mean
Learning rate	0.001	0.001	0.001
Num. epochs	200	200	200
Task	Binary	Multiclass	Regression

Table 4: Configurations used for the graph neural network baselines in Table 2.

B.4 Compute details

In terms of computing, the experiments were run on a HPC cluster with Nvidia P100 GPUs and 14-core Intel Broadwell 2.4 GHz CPUs.